Electric modulation of conduction in MAPbBr$_3$ single crystals

Shanming Ke,[a] *Shangyu Luo,*[a] *Jinhui Gong,*[a] *Liwen Qiu,*[a] *Renhong Liang,*[a] *Yangbo Zhou,*[a]

Bingcheng Luo,[b] *Baochang Cheng,*[a] *Li Wang,*[a,*] *Longlong Shu*[a,*]

[a] School of Materials Science and Engineering, Nanchang University, Nanchang 330031, People's Republic of China

[b] State Key Laboratory of Solidification Processing, Northwestern Polytechnical University, Xi'an 710072, People's Republic of China

Corresponding Author: *E-mail: wl@ncu.edu.cn (L.W.), *E-mail: llshu@ncu.edu.cn (L.S.)

■ **ABSTRACT**

The resistive switching (RS) mechanism of hybrid organic-inorganic perovskites is an open question until now. Here, a switchable diode-like RS behavior in MAPbBr$_3$ single crystals using Au (or Pt) symmetry electrodes is reported. Both the high resistance state (HRS) and low resistance state (LRS) are electrode-area dependent and light responsive. We propose an electric-field-driven inner p-n junction accompanied by an interface trap-controlled SCLC mechanism to explain this switchable diode-like RS behavior in MAPbBr$_3$ single crystals.

Keywords: resistive switching, rectifying behavior, hybrid organic-inorganic perovskites, p-n structure

1. Introduction

Currently, hybrid organic-inorganic perovskites (HOIPs) have been dynamically investigated for the potential applications in solar cells [1], light-emitting diodes [2], photodetectors [3], lasers [4] and transistors [5]. For perovskite solar cells, a large electrical hysteresis in current-voltage (*I-V*) curves has been frequently reported, which is generally attributed to ferroelectricity [6], charge trapping [7], or ion migration [8]. Although the large hysteresis needs to be eliminated in optoelectric devices, this phenomenon inspired the observation of resistive switching (RS) behavior in hybrid perovskite films [9-16], which is exploited for multilevel data storage.

RS phenomena have attracted a very large interest in the last years. Generally, the RS devices with a capacitor-like structure could be switched by an external bias to two different resistance states, a high resistance state (HRS) and a low resistance state (LRS). Yoo *et al.* [9] reported the RS behavior for the first time in $MAPbI_{3-x}Cl_x$ (MA is shorted for $CH_3NH_3^+$) perovskite films, and proposed a mechanism based on the trap-controlled space-charge-limited conduction (SCLC). Recently, interface-type RS was observed in $Au/MAPbBr_3/ITO$ by Guan *et al.* [10] They proposed that the switching mechanism could be due to the migration of MA vacancies and the modification of the interfacial Schottky barrier. The filamentary-type RS has also been observed in several other works on $MAPbI_3$-based films, where the conducting filaments were attributed to the migration of anions defects [11-13] or Ag ions from the redox reactions of Ag electrode [14,15]. Moreover, the RS behavior of HOIPs could be strongly influenced by illumination. Chai *et al.* [16] found that the set voltage could be greatly lowered under light illumination in $MAPbI_3$-based RS devices. However, in a previous work [17], we found no meaningful RS behavior in an individual $MAPbI_3$ nanowire unless under light

illumination. These results clearly indicate that there remain many open questions regarding RS phenomena and switching mechanism in HOIP-based RS devices.

In this work, $MAPbBr_3$ single crystal was chose for the conduction study, because $MAPbBr_3$ is non-polar (centrosymmetric) [18] and therefore ferroelectricity could be excluded, while the influence of grain boundaries can also be ignored. Compared with polycrystalline thin films [19,20], $MAPbX_3$ single crystals present lower trap density and much better environmental stability, which can be considered as an ideal platform for investigating their intrinsic physical properties. The electric-field-driven resistance switching accompany by a diode-like behavior was produced in the $Au/MAPbBr_3/Au$ structure. The diode-like switchable effect can be explained by the formation of reversible p-n junctions induced by ion immigration in the crystals. The area-proportional conduction indicates an interface-type RS behavior, which is related to the charge trapping/detrapping process at the interface.

2. Experimental Section

The $MAPbBr_3$ single crystals were prepared from solution by inverse temperature crystallization (ITC) method [18]. The raw materials methylammonium bromide (CH_3NH_3Br, 99.5%), lead bromide ($PbBr_2$, 99.9%), N, N-dimethylformamide (DMF, 99%), and dimethylsulfoxide (DMSO, 99%) were used as received. CH_3NH_3Br and $PbBr_2$ with a molar ratio of 1:1 were dissolved in DMSO-DMF (7:3 by volume) to form a solution, and $MAPbBr_3$ was crystallized at the temperature from 60 °C to 100 °C with a heating rate of 0.2 - 0.5 °C/h.
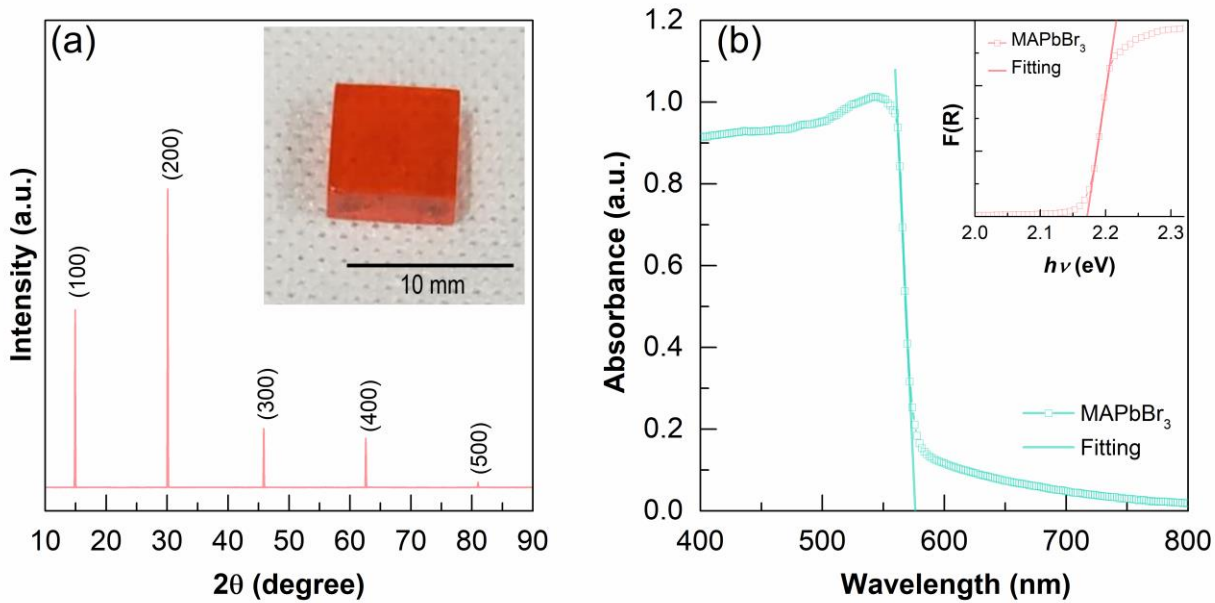
An X-ray diffractometer (XRD, PANalytical X'pert) was used for phase identification at room temperature. The absorption spectra were measured in the wavelength range of 400–800 nm using an UV spectrometer (SpectraPro-275, Acton Research Corporation). Au (100 nm) was used as the electrode for electrical characteristics with different sizes. The current-voltage (*I-V*)

measurements were carried out using a semiconductor analyzer (FS380, Platform Design Automation, Inc.) assisted with a probe station (Lakeshore TTPX). To avoid the influence of the environmental gases and moisture [21], the samples were kept in a vacuum chamber for electrical characteristics with a pressure of 10^{-4} mbar.
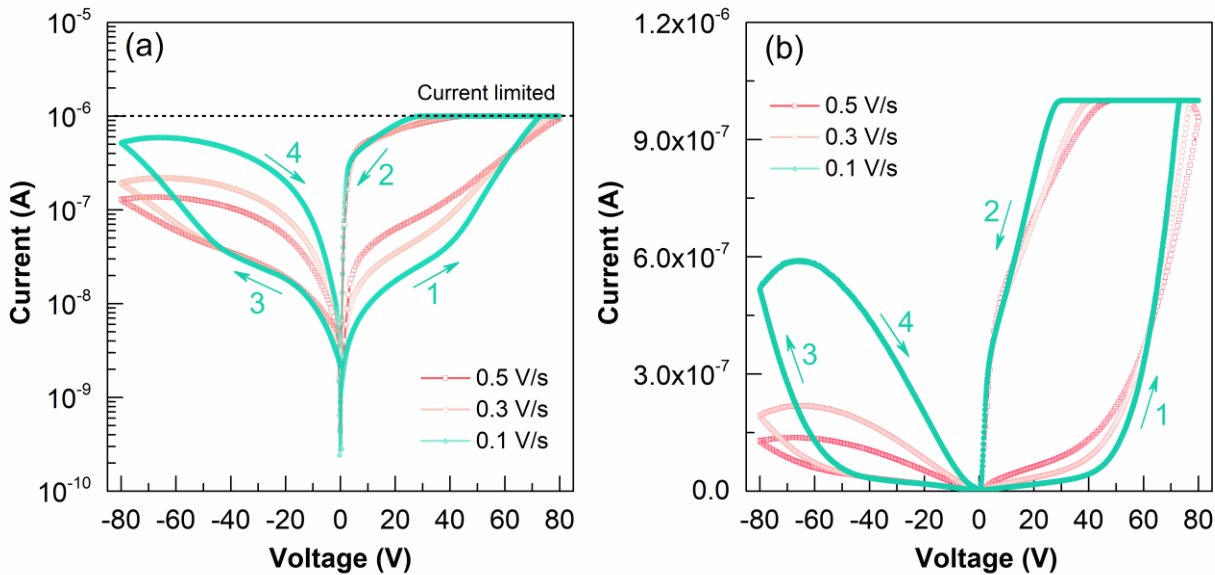
3. Results and Discussion

The inset of Figure 1a shows an optical image of an MAPbBr$_3$ single crystal with dimensions of ~ 6×7×2 mm^3. Figure 1a presents the typical XRD 2θ scan data of the MAPbBr$_3$ single crystal at room temperature. The crystal adopts a pure cubic phase with good crystallization and high quality. The absorbance of MAPbBr$_3$ (Figure 1b) shows a clear band edge cutoff with no excitonic signature, which suggests a minimal number of in-gap defect states [22]. The optical band gap of MAPbBr$_3$ could be determined to be 2.17 eV by extrapolating the linear region of the absorption edge to the energy-axis intercept, which is similar to the other reports [18].

Figure 2 shows the dark current of the Au/MAPbBr$_3$/Au structure with different scanning rates and directions in two different scale. The arrows in the figure depict the bias scanning directions. The sequence of voltage sweep is 0 → +80 V → 0 → -80 V → 0, where the voltage is termed as positive when the top electrode is positively biased. A clear switchable diode-like RS behavior is observed in Figure 2, which is quite different from the previous work on HOIP thin film devices [9-16]. In most of these films, only resistive switching but no diode-like behavior was mentioned. The diode direction can be switched during the sweep process in the dark. During the scan path 2, the device switches to the LRS. When the scan direction reverses in the path 3 the current abruptly decrease and the device switches to HRS. The on/off ratio of the dark current is ~ 54 at a bias of +10 V.

Figure 1. (a) XRD and (b) absorption spectra of MAPbBr$_3$ single crystals. Inset: (a) image of one of the measured crystals grown from solution; (b) absorbance versus photon energy and the determined band gap E_g.
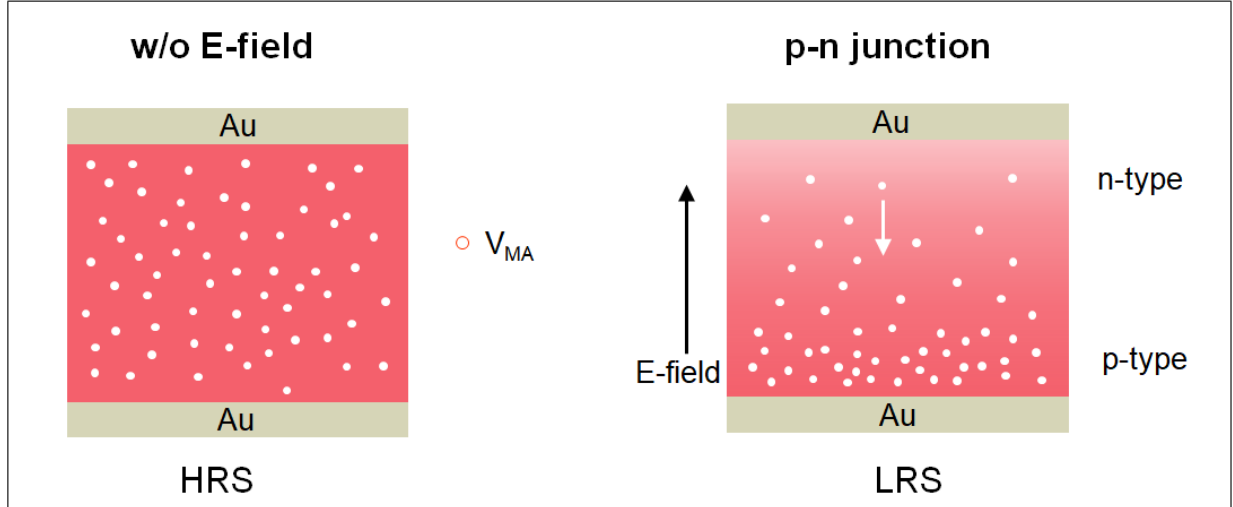

Figure 2. Current-voltage traces. *I-V* curves of an Au/MAPbBr$_3$/Au device in (a) log-scale and (b) normal-scale in the dark with different scanning rates. All the measurements were conducted at room temperature in a vacuum chamber.

We now focus on the origin of the switchable diode-like resistive switching. The switchable diode-like RS generally occurs in ferroelectric devices [23], where the barrier height at the ferro/electrode interface could be controlled by the switchable ferroelectric polarization. Actually, the switchable diode behavior has been observed in $Au/MAPbI_3/ITO$ thin film devices, which results in a giant switchable photovoltaic effect under illumination [24]. According to the proposed mechanism in refs. 28 and 29, since $MAPbBr_3$ is a non-ferroelectric, the switchable diode can be understood in terms of the defects electromigration process, as shown in Figure 3. It is known that many types of point defects have been reported in the HOIPs, such as V_{Pb}, V_{Br}, V_{MA}, etc. Positively-charged Br vacancy (V_{Br}) can lead to n-type doping, whereas negatively charged Pb and MA vacancies (V_{Pb} and V_{MA}) result in p-type doping [25]. Provided that the defects are mobile charges, they can move through the sample under electric fields to find a new thermodynamic equilibrium. For instance, V_{MA} can move and pile up near the bottom surface for negative bias conditions. Thus, the top surface region acquires n-type carriers, whereas the region near the bottom electrode becomes p-type. Yuan *et al.* have reported a direct observation of MA^+ ion and V_{MA} migration under a bias field [26]. The reversible p-n structures induced by ion drift has also been confirmed in HOIPs [24].

Noting that the rectifying p-n junction created through the asymmetric distribution of charged defects is also believed to induce of a RS behavior directly [27]. The low resistance state (LRS) can be attributed to the creation of p-n junction. By applying an opposite electric field, the inhomogeneous donor/or acceptor distribution can be reversed to an evenly distributed insulating state (HRS). For a full sweep cycle (Figure 2a), scan path 1 (HRS) and 4 (LRS) are quite sensitive to the scanning rate, which just reveals the defects electromigration process. Path 1 displays the forming process of the p-n structure from an evenly defect distribution. After the
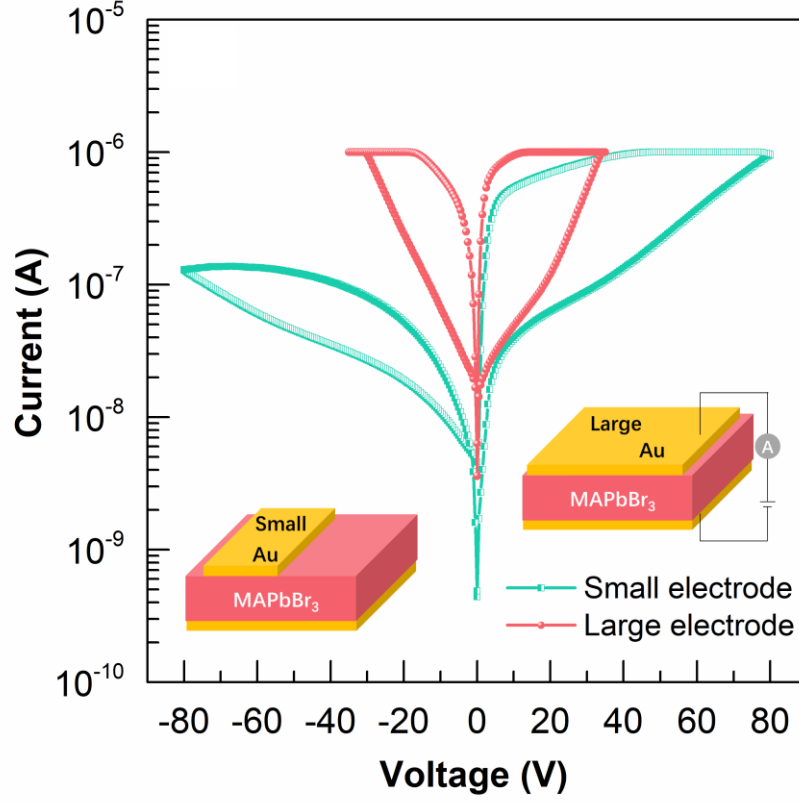
creation of inner p-n junction, the Au/MAPbBr$_3$/Au structure shows a low resistance state and its current is then not sensitive to scan speed (path 2).
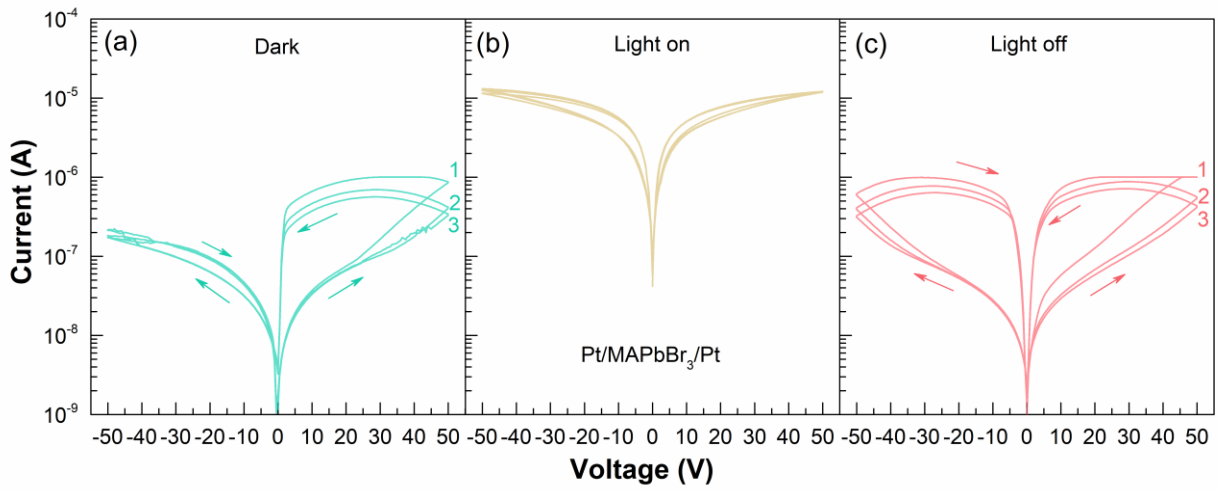

Figure 3. Schematic diagram describing the rectifying behavior of electronic states in MAPbBr$_3$ single crystal. Negatively charged V$_{MA}$ is focused here, and the inclusion of other defects does not alter the conclusion. The MA vacancies respond to electric field. In a negative field (bottom to up), MA vacancies are moving downward and accumulating near the bottom surface and are frozen when the field is turned off. As a result, a state with p-type carriers is realized; the opposite region becomes a n-type conductor.

Notwithstanding, the p-n junction scenario cannot solely explain the asymmetrical and electrode-area dependent *I-V* results. Figure 4 displays the RS behavior of an Au/MAPbBr$_3$/Au device with different size of up-electrode. It can be seen that both the HRS and LRS are electrode area-dependent, which could be regarded as a fingerprint of an interface-type resistive switching [23]. Furthermore, as shown in Figure 2, the two hysteresis loops in one sweep cycle (path 1 to path 4) obtained under forward and reverse biases are asymmetrical, which further implies the interface-type RS nature. These asymmetrical loops can be observed more

conspicuously in a Pt/MAPbBr$_3$/Pt device (see Figure 5a). These results imply that the interface conduction also plays an important role in the switchable diode-like resistive switching.

Figure 4. *I-V* curves of an Au/MAPbBr$_3$/Au device in the dark with different up-electrode area.

Figure 5. *I-V* curves of an Pt/MAPbBr$_3$/Pt device (a) in the dark, (b) under light illumination (1500 LUX) and (c) subsequent light off.
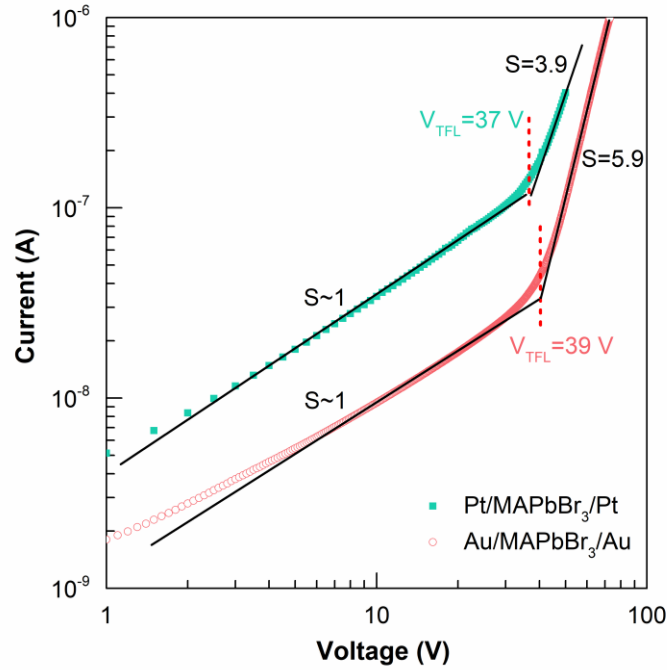
The interface-type RS phenomenon has been explained by various conduction mechanisms such as trap-controlled SCLC, Schottky emission, and hopping conduction [9,28]. It was previously reported that Au and Pt form an Ohmic contact with HOIPs [22,29]. Then the interfacial Schottky barrier [10,16] scenario should be excluded in our case. To further understand the conduction mechanism, we replotted the *I-V* curves of HRS in a log-log scale as shown in Figure 6. Two regions were evident in the HRS curves. At low voltages, the *I-V* response was ohmic ($I \infty V$). At high fields, the current exhibited a rapid non-linear rise and signaled the transition onto the trap-filled limit (TFL) regime, in which all the available trap states were filled by the injected carriers [30]. The *I-V* response of the trap-filled SCLC is marked by a steep increase in current ($I \infty V^{n>3}$). The onset voltage V_{TFL} (V_{TFL} =37 *V* for Pt electrodes and 39 *V* for Au electrodes) is typically linearly proportional to the density of trap states as follows [31],
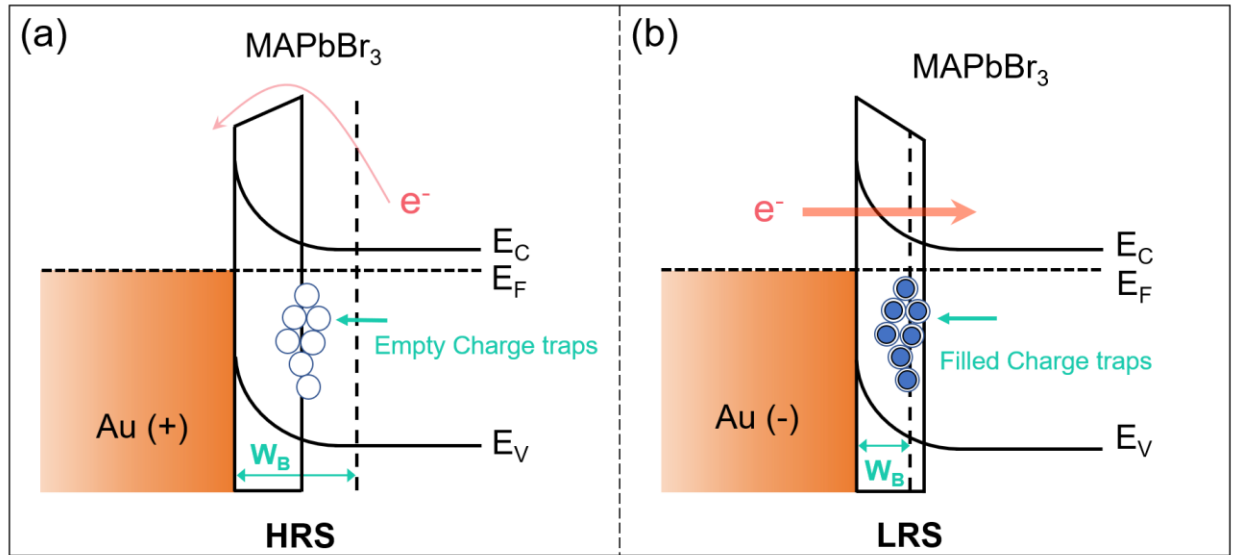
$$V_{TFL} = 8en_t d^2/9\varepsilon\varepsilon_0 \qquad (1)$$

Where n_t is the density of trap states, *d* is the thickness of the sample, ε is the dielectric constant (here we use 25 for MAPbBr$_3$) [32], and ε_0 is the vacuum permittivity. Correspondingly, it could be found that our MAPbBr$_3$ single crystals have a trap density of $\sim 1.5 \times 10^{12}$ cm^{-3}.

According to the above area-dependent results, we propose partially an interface RS mechanism based on charge trapping/detrapping at the perovskite/Au (or Pt) interfacial trapping centers. As illustrated in Figure 7, the resistance is determined by the filling state of the interface charge traps. Charge traps could be introduced during the crystal growth procedure and can thus be controlled for the RS properties. At the initial state, the traps are empty and leads to the HRS by increasing the tunneling barrier width. If all the traps are filled, the injected carriers can move freely into the perovskite crystals and then lead to a low resistance state.
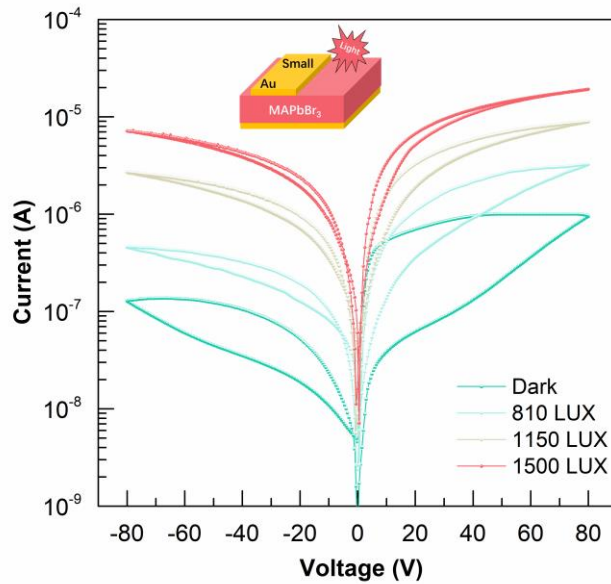
Figure 6. The high resistance state of MAPbBr$_3$ single crystals with Au and Pt electrodes in a log-log scale. Characteristic *I-V* traces showing two different regimes. A linear ohmic regime ($I \propto V$) is followed by the trap-filled regime ($I \propto V^{n>3}$).

Figure 7. (a, b) the trap/detrap and tunneling of electrons. When a positive voltage is applied to the electrode, this results in charge trapping, narrowing of the interfacial barrier width and induces an HRS-to-LRS switching.

Interestingly, the trap states at the perovskite/Pt (or Au) interface can be modulated by light absorption. Figure 5a, b, and c show the *I-V* curves of a Pt/MAPbBr$_3$/Pt device in the dark, under light illumination and subsequent light off, respectively. For the initial measurement in the dark, the switching loop under reverse bias is severely restricted, which means the traps were not fully filled in this sweep process. After light illumination, some of the interface traps are "activated" and then induce an obviously resistance switching behavior (Figure 5c). Figure 8 illustrates the evolution of RS behavior of Au/MAPbBr$_3$/Au device under light illumination with different intensity. Under the light illumination, both the HRS and LRS currents increase due to the existence of photocurrent. The resistive switching loops became narrower than the dark case, and wore off eventually. The results of both area-dependent and light-responsive experiments exclude the possible of metallic filaments mechanism for the observed RS behavior.

Figure 8. *I-V* curves of an Au/MAPbBr$_3$/Au device under light illumination with selected power density.

On the other hand, the interface charge trapping/detrapping cannot either solely explain the switchable diode-like RS behavior. Because the interface charge trapping state cannot change obviously when the voltage is just reversed, which cannot induce a diode-like behavior. It is worth noting that the trap-controlled SCLC could be used to describe not only the conduction of an interface charge trapping/detrapping process, but also the defects electromigration process [24,27]. The aforementioned switchable diode-like RS behavior can be then explained by the formation of an electric-field-driven p-n junction accompanied by a trap-controlled SCLC at the electrode-perovskite interface. The resistance state (HRS and LRS) depends on the synergy between the inner p-n junction and the interface.

4. Conclusions

In summary, a switchable diode-like RS behavior was observed in MAPbBr$_3$ single crystals using Au (or Pt) symmetry electrodes. The dependence of the surface barrier on the interface trap filling level plays a vital role on the resistance switching. The emptied traps cause a wide tunneling barrier height and correspondingly cause a high resistance state. When the injected carriers fill the traps in the surface space charge region, the barrier was narrowed and the device switches to the LRS. During the interface trap filling or emptying processes, the charged defects also migrate under applying a bias and lead to a reversible p-n structure in the crystal.

Declaration of Competing Interest

The authors declare that they have no known competing financial interests or personal relationships that could have appeared to influence the work reported in this paper.

Acknowledgments

References

[1] Huang C, Lin P, Fu N, Liu C, Xu B, Sun K, Wang D, Zeng X, Ke S. Facile fabrication of highly efficient ETL-free perovskite solar cells with 20% efficiency by defect passivation and interface engineering, *Chem Commun* 2019, **55**: 2777-2780.

[2] Lin K, Xing J, Quan LN, Arquer de F, Gong X, Lu J, Xie L, Zhao W, Zhang D, Yan C, Li W, Liu X, Lu Y, Kirman J, Sargent EH, Xiong Q, Wei Z. Perovskite light-emitting diodes with external quantum efficiency exceeding 20 per cent, *Nature* 2018, **562**: 245-248.

[3] Ma C, Shi Y, Hu W, Chiu MH, Liu Z, Bera A, Li F, Wang H, Li LJ, Wu T. Heterostructured $WS_2/CH_3NH_3PbI_3$ photoconductors with suppressed dark current and enhanced photodetectivity, *Adv Mater* 2016, **28**: 3683-3689.

[4] Zhu H, Fu Y,. Meng F, Wu X, Gong Z, Ding Q, Gustafsson MV, Trinh MT, Jin S, Zhu XY. Lead halide perovskite nanowire lasers with low lasing thresholds and high quality factors, *Nat Mater* 2015, **14**: 636-642.

[5] Long M, Zhang T, Chai Y, Ng CF, Mak TCW, Xu J, Yan K. Nonstoichiometric acid–base reaction as reliable synthetic route to highly stable $CH_3NH_3PbI_3$ perovskite film, *Nat Commun* 2016, **7**: 13503.

[6] Rakita Y, Bar-Elli O, Meirzadeh E, Kaslasi H, Peleg Y, Hodes G, Lubomirsky I, Oron D, Ehre D, Cahen D. Tetragonal $CH_3NH_3PbI_3$ is ferroelectric, *Proc Natl Acad Sci* 2017, **114**: E5504-E5512.

[7] Snaith HJ, Abate A,. Ball JM, Eperon GE, Leijtens T, Noel NK, Stranks SD, Wang JTW, Wojciechowski K, Zhang WJ. Anomalous hysteresis in perovskite solar cells, *J Phys Chem Lett* 2014, **5**: 1511-1515.

[8] Azpiroz JM, Mosconi E, Bisquert J, Angelis De F. Defect migration in methylammonium lead iodide and its role in perovskite solar cell operation, *Energy Environ, Sci* 2015, **8**: 2118-2127.

[9] Yoo EJ, Lyu M, Yun JH, Kang CJ, Choi YJ, Wang L. Resistive switching behavior in organic–inorganic hybrid $CH_3NH_3PbI_{3-x}Cl_x$ perovskite for resistive random access memory devices, *Adv Mater* 2015, **27**: 6170-6175.

[10] Guan X, Hu W, Haque MA, Wei N, Liu Z, Chen A, Wu T. Light-Responsive ion-redistribution-induced resistive switching in hybrid perovskite schottky junctions, *Adv Funct Mater* 2018, **28**: 1704665.

[11] Gu C, Lee JS. Flexible hybrid organic–inorganic perovskite memory, *ACS Nano* 2016, **10**: 5413-5418.

[12] Choi J, Park S, Lee J, Hong K, Kim DH, Moon CW, Park GD, Suh J, Hwang J, Kim SY, Jung HS, Park NG, Han S, Nam KT, Jang HW. Organolead halide perovskites for low operating voltage multilevel resistive switching, *Adv Mater* 2016, **28**: 6562-6567.

[13] Hwang B, Lee JS. A strategy to design high-density nanoscale devices utilizing vapor deposition of metal halide perovskite materials, *Adv Mater* 2017, **29**: 1701048.

[14] Sridharan A, Noe NK, Hwang H, Hafezian S, Rand BP, Kena-Cohen S. Enhanced endurance organolead halide perovskite resistive switching memories operable under an extremely low bending radius, *ACS Appl Mater Inter* 2017, **9**: 30764-30771.

[15] Yoo E, Lyu M, Yun JH, Kang C, Choi Y, Wang LJ. Bifunctional resistive switching behavior in an organolead halide perovskite based $Ag/CH_3NH_3PbI_{3-x}Cl_x/FTO$ structure, *J Mater Chem C* 2016, **4**: 7824-7830.

[16] Zhou F, Liu Y, Shen X, Wang M, Yuan F, Chai Y. Optoelectronic $CH_3NH_3PbI_{3-x}Cl_x$ memory with integrated sensing and logic operations, *Adv Funct Mater* 2018, **28**: 1800080.

[17] Hong Z, Zhao J, Li S, Cheng B, Xiao Y, Lei S. Tunable hysteresis behaviour related to trap filling dependence of surface barrier in an individual $CH_3NH_3PbI_3$ micro/nanowire, *Nanoscale* 2019, **11**: 3360-3369.

[18] Liu Y, Yang Z, Cui D, Ren X, Sun J,. Liu X, Zhang J, Wei Q, Fan H, Yu F, Zhang X, Zhao C, Liu S. Two-Inch-Sized perovskite $CH_3NH_3PbX_3$ (X = Cl, Br, I) crystals: growth and characterization, *Adv Mater* 2015, **27**: 5176-5183.

[19] Mallik AK, Bysakh S, Roy S, Roy S, Mendes JC, Gracio J, Datta S. Property mapping of polycrystalline diamond coatings over large area, *J Adv Ceram* 2014, **3**: 56-70.

[20] Zhang CS, Hu DL, Gu H, Xing JJ, Xiong P, Wan DY, Gao, YF. Crystallization and inter-diffusional behaviors in the formation of VO2(B) thin film with layered W-doping, *J Adv Ceram* 2017, **6**: 196-206.

[21] Shu L, Ke S, Fei L, Huang W, Wang Z, Gong J, Jiang X, Wang L, Li F, Lei S, Rao Z, Zhou Y, Zheng R, Yao X, Wang Y, Stenge M, Catalan G, Photoflexoelectric effect in halide perovskites, *Nat Mater* 2020, **19**: 605-609.

[22] Fang HH, Adjokatse S, Wei H, Yang J, Blake GR, Huang J, Even J, Loi MA, Ultrahigh sensitivity of methylammonium lead tribromide perovskite single crystals to environmental gases, *Sci Adv* 2016, **2**: e1600534.

[23] Shi D, Adinolfi V, Comin R, Yuan M, Alarousu E, Buin A, Chen Y, Hoogland S, Rothenberger A, Katsiev K, Low trap-state density and long carrier diffusion in organolead trihalide perovskite single crystals, *Science* 2015, **347**: 519-522.

[24] Tian J, Tan Z, Fan Z, Zheng D, Wang Y, Chen Z, Sun F, Chen D, Qin M, Zeng M, Depolarization-field-induced retention loss in ferroelectric diodes, *Phys Rev Appl* 2019, **11**: 024058.

[25] Xiao Z, Yuan Y, Shao Y, Wang Q, Dong Q, Bi C, Sharma P, Gruverman A, Huang J, Giant switchable photovoltaic effect in organometal trihalide perovskite devices, *Nat Mater* 2015, **14**: 193-198.

[26] Game OS, Buchsbaum GJ, Zhou Y, Padture NP, Kingon A, Ions matter: description of the anomalous electronic behavior in methylammonium lead halide perovskite devices, *Adv Funct Mater* 2017, **27**: 1606584.

[27] Yuan Y, Chae J, Shao Y, Wang Q, Xiao Z, Centrone A, Huang J, Photovoltaic switching mechanism in lateral structure hybrid perovskite solar cells, *Adv Energy Mater* 2015, **5**: 1500615.

[28] Yang CH, Seidel J, Kim SY, Rossen PB, Yu P, Gajek M, Chu YH, Martin LW, Holcomb MB, He Q, Maksymovych P, Balke N, Kalinin SV, Baddorf AP, Basu SR, Scullin ML, Ramesh R, Electric modulation of conduction in multiferroic Ca-doped $BiFeO_3$ films, *Nat Mater* 2009, **8**: 485-493.

[29] Bagdzevicius S, Maas K, Boudard M, Burriel MJ, Interface-type resistive switching in perovskite materials, *J Electroceram* 2017, **39**: 157-184.

[30] Saidaminov MI, Adinolfi V, Comin R, Abdelhady AL, Peng W, Dursun I, Yuan M, Hoogland S, Sargent EH, Bakr OM, Planar-integrated single-crystalline perovskite photodetectors, *Nat Commun* 2015, **6**: 8724.

[31] Lampert MA, Mark P, Current injection in solids, *New York, NY : Academic Press* 1970.

[32] Lian Z, Yan Q, Gao T, Ding J, Lv Q, Ning C, Li Q, Sun Jl, Perovskite $CH_3NH_3PbI_3(Cl)$ Single Crystals: Rapid Solution Growth, Unparalleled Crystalline Quality, and Low Trap Density toward 108 cm^{-3}, *J Am Chem Soc* 2016, **138**: 9409-9412.